IEEE Access
Multidisciplinary ⋮ Rapid Review ⋮ Open Access Journal

Received 26 August 2023, accepted 15 September 2023, date of publication 4 October 2023, date of current version 10 October 2023.

Digital Object Identifier 10.1109/ACCESS.2023.3321804

RESEARCH ARTICLE

Data-Driven Adaptive Automated Driving Model in Mixed Traffic

PRANAV RAMSAHYE[1], SUSILAWATI SUSILAWATI[1], (Member, IEEE), CHEE PIN TAN[2], (Senior Member, IEEE), AND MD ABDUS SAMAD KAMAL[3], (Senior Member, IEEE)

[1]Department of Civil Engineering, Monash University Malaysia, Bandar Sunway 47500, Malaysia
[2]Department of Robotics and Mechatronics Engineering, Monash University Malaysia, Bandar Sunway 47500, Malaysia
[3]Graduate School of Science and Technology, Gunma University, Kiryu 376-8515, Japan

Corresponding authors: Md Abdus Samad Kamal (maskamal@ieee.org) and Susilawati Susilawati (susilawati@monash.edu)

This work was supported in part by the Ministry of Education Malaysia under the Fundamental Research Grant Scheme (FGRS) under Project FRGS/1/2019/TK01/MUSM/03/1, and in part by the Japan Society for the Promotion of Science (JSPS) Grant-in-Aid for Scientific Research (C) under Grant 23K03898.

ABSTRACT The interplay between Connected Automated Vehicles (CAVs) and Human-driven Vehicles (HDVs) in mixed traffic environments is often presumed to influence the behavior of the other, and the dynamic impacts of such interplay on traffic flows is a critical aspect that is absent in most existing studies. This study employs a data-driven optimization approach to model the driving behavior of Connected Automated Vehicles (CAV) in mixed traffic and investigates the impact of CAVs on overall traffic performance. Specifically, considering a scenario of a gradual increase in the penetration of CAVs in the conventional traffic stream, currently dominated by Human-driven vehicles (HDV), four possible car-following configurations are identified where a CAV has to behave differently. Regarding such configurations, existing car-following and lane-changing models of CAVs are tuned using a Lipschitzian optimization algorithm and a local search method with data obtained from the WAYMO Open Dataset. The developed driving model of CAVs is used to simulate mixed traffic on a freeway section attached to an on-ramp, which often induces traffic bottlenecks. Under varying market penetration of CAVs, traffic performances, including travel time, throughput, and string stability, are compared with conventional traffic. The findings suggest significant improvements at a network level, for example, by delaying and dampening shockwaves. However, on an individual level, CAVs feel hindered by the slower-moving HDVs.

INDEX TERMS Connected automated vehicles, freeway on-ramp, mixed traffic microsimulation, model optimization, Waymo open dataset.

I. INTRODUCTION

The emerging sector of automated vehicles, expected to represent a $7 trillion opportunity by 2050 [1], has garnered recent, widespread attention as its potential societal, economic, and environmental advantages have become widely coveted. As companies race to become leaders in this new industry, the question of how automated vehicles will influence and redefine mixed traffic dynamics must be answered - particularly during the transitional phase that will occur as automated vehicles gradually seize market share from conventional human-driven vehicles.

A relatively new area of study, conclusive and extensive literature on automated vehicles has yet to be published [2], and several research gaps remain to be discussed before the global deployment of these vehicles. Currently, the assumptions that inform the objectives and methods in available literature on automated driving models in mixed traffic vary significantly. This is partly due to the interdisciplinary nature of this research direction, and further, the lack of field data has made the calibration of automated driving models difficult. Currently, microscopic models are calibrated from the NGSIM dataset [3], [4], which can reasonably only be

The associate editor coordinating the review of this manuscript and approving it for publication was Wei Wei.

© 2023 The Authors. This work is licensed under a Creative Commons Attribution-NonCommercial-NoDerivatives 4.0 License.
For more information, see https://creativecommons.org/licenses/by-nc-nd/4.0/

applied to human driving or synthetic data [5], which is often unable to reflect real-world conditions. Moreover, Human-driven Vehicles (HDVs) and Connected Automated Vehicles (CAVs) have distinct driving mechanisms, and thus interact and respond differently to each other's behavior. These interactions simply describe how the presence of a CAV affects the behavior of an HDV, and vice versa. In mixed traffic conditions, there are four possible car-following interactions: (1) CAV follower and CAV leader; (2) CAV follower and HDV leader; (3) HDV follower and CAV leader; and (4) HDV follower and HDV leader.

Most studies of automated driving behavior have only focused on one-dimensional analysis of traffic flow, namely, car-following in the same lane. Very few have attempted to include lane-changing maneuvers into their microscopic traffic model and assessed their impacts on mixed traffic flow [6], [7], despite lane-changing being associated with stop-and-go oscillations that propagate upstream and eventually affect traffic throughput [8], [9]. These oscillations occur during a lane change because of sudden, responsive changes in the car-following behavior of the surrounding vehicles, including the abrupt deceleration of the new follower in the target lane [10], [11].

Typically, a lane change is completed in two stages: (1) anticipation, which occurs when the subject vehicle prepares to move into a target lane, and (2) relaxation, which occurs when the subject has successfully merged into the target lane and begins to follow its new leader steadily. As a subject vehicle transitions from the anticipation stage to the relaxation stage, there is a change in the car-following interactions of the surrounding vehicles involved in the lane change. Some recent studies have discussed automated driving during lane-changing but are largely focused on the relaxation stage, which is regarded as the most significant cause of capacity drops [12], [13]. As a result, there is less clarity in a microscopic traffic model that can describe the surrounding vehicles' responses to a lane change during the anticipation stage.

This in turn raises three research questions: (a) How can a two-dimensional microscopic traffic model depict interactions between two vehicle types during both car-following and lane-changing behaviors? (b) How can inter-vehicular interactions be quantitatively optimized to facilitate reliable results? (c) Can this new microscopic traffic model effectively incorporate inter-vehicular interactions to obtain traffic performance results for mixed traffic?

To address the research questions above, this study develops a microscopic traffic model, which quantifies the interactions between CAVs and HDVs during car-following behavior [14], [15] and, importantly, incorporates these interactions into the lane-changing model during both the anticipation and relaxation stages. This is achieved by describing the interactions through car-following model parameters and by using a lane-changing model that is based on the longitudinal model. Therefore, the proposed model combines the IDM car-following algorithm and the MOBIL lane-changing algorithm to form a new microscopic traffic model. Further, each interaction is optimized to ensure accurate mixed traffic performance results.

The main contributions of this study are summarized as follows:

- To develop a two-dimensional model that describes both car-following and lane-changing behavior by considering inter-vehicular interactions. This is critical due to the inherently different control strategies of CAVs and HDVs [16]. Those interactions are transferred to the lane-changing model during both the anticipation and relaxation stages of the lane change.
- To optimize the microscopic model, utilizing a Lipschitzian Optimization algorithm combined with a local search method on trajectory data from the Waymo Open dataset to rapidly identify a global optimum solution for each possible car-following interaction in mixed traffic.
- To investigate the network performance of multilane traffic at varying CAV penetration in terms of travel time, throughput, and stability within a test bed consisting of an on-ramp attached to a three-lane freeway section. This traffic environment is representative of typical bottleneck situations, which have received limited attention in mixed traffic [17].

This paper is organized as follows. The following section provides an overview of the relevant microscopic studies of automated vehicles and highlights key gaps. Section III then presents the proposed microscopic traffic model at an on-ramp and calibrates the model parameters for the potential interactions. Section IV analyses and discusses key findings, and the final section concludes the paper and suggests future research direction.

II. RELATED WORK

Many studies have provided insight into the advantages of pure CAV traffic [18], [19], [20], [21], [22], which is the long-term vision of traffic automation. However, the traffic flow dynamics of mixed autonomy remain under-explored, and yet, this will be the reality of traffic in the near future as we gradually transition into fully automated driving. Therefore, this study focuses on investigating the aspects of mixed autonomy that are expected in the short term. More specifically, we explore how HDVs and CAVs interact with and influence each other. In mixed traffic, where CAVs and HDVs co-exist, car-following algorithms may be classified into four interactions as follows: [23], [24]

- CAV leader and CAV follower – When a CAV follows another CAV, the vehicles can exchange real-time information on distance gaps or speed differences via Vehicle-to-Vehicle (V2V) communication. Thus, the movement of the follower is synchronized with its leader. This type of behavior is known as Cooperative Adaptive Cruise Control (CACC).

- CAV follower and HDV leader – When a CAV follows an HDV, there is a degradation in the CAV's ability to synchronize its behavior to its leading HDV because the vehicles cannot communicate with each other. This is known as Adaptive Cruise Control.
- HDV follower and CAV leader – There are two schools of thought regarding this interaction. Most studies assume that an HDV is unable to differentiate between a leading CAV or HDV and would therefore treat the CAV as an HDV. On the other hand, if the HDV were able to differentiate between a CAV and an HDV, the HDV would treat the CAV as a different vehicle type and adjust its movement accordingly. For example, these studies have suggested that an HDV will tend to imitate the shorter time headway of a CAV [25], [26].
- HDV follower and HDV leader – This interaction has been thoroughly investigated and documented. Due to the fickleness of human driving, this is the least advantageous interaction for optimal traffic performance.

Several algorithms have been proposed to describe the automated driving behavior of CACC-equipped systems [27], [28], [29], [30]. However, the presence of HDVs in mixed traffic streams is likely to impact the behavior of CAVs [17], in part due to a loss of communication, which degrades the CAV's following behavior from CACC to ACC. Currently, the literature regarding the modeling of inter-vehicular interactions in mixed traffic is scarce, and the assumptions and methods vary significantly [31]. Therefore, it is unclear how CAVs and HDVs may influence each other due to a lack of complexity in terms of the traffic ecosystem investigated in existing studies. Most current research on mixed traffic focuses on two polar scenarios – where a single CAV is employed amongst a dense number of HDVs, or where many CAVs are simulated with no interaction with human-controlled counterparts. Much less emphasis has been on the far more significant yet challenging transition between these two extremes due to the current uncertain and complex interactions between the two vehicle types. However, it is exactly this type of hybrid human-machine subspace (or mixed autonomy) that deserves attention [32].

Some recent mixed traffic microsimulation works have found that the throughput of a freeway section will increase at high CAV penetration rates, causing smaller queue lengths and congestion areas [33], [34]. In this vein, Zhou and Laval [35] surveyed the longitudinal control of CAVs and also report the benefits on traffic congestion. This was assumed to be caused by CAVs' ability to adopt smaller time headway spacing. However, since there was no distinction made between the CAV's time headway with a leading HDV and a leading CAV, the results may be overestimated as, in reality, we could expect a longer time headway when the leader is an HDV. Moreover, the studies have not explored the influence of lane-changing behavior on local capacity drops and congestion areas as they dealt solely with single-lane freeways with no disturbances. Other relevant studies have focused on the environmental advantages that CAVs could offer, reporting lower emissions of greenhouse gases due to smoother acceleration profiles [20], [36]. These findings were based on straight single-lane freeways with no added disturbances and therefore, cannot dissect the impact of lane-changing on acceleration rates. Lane-changing leads to imperfect acceleration and deceleration, which subsequently increases traffic speed heterogeneity and negatively affects traffic performance. The prevalent research focus on car-following only has therefore created a research gap in the industry on the effects of lane-changing in mixed traffic flow.

As researchers became more aware of the nuances of traffic behavior in simple scenarios, studies have refocused their attention on some complex study environments by including arterials and secondary urban roads in the traffic environment under investigation [37], [38] or by exploring signalized [39], [40] and non-signalized [41] intersections. Further, researchers have refocused their attention on bottleneck situations, such as freeways with on/off-ramps, as comprehensively reviewed by Zhu et al. [42]. However, most existing studies at on/off-ramps are either based on single-lane analysis [43], [44] or on an oversimplified traffic composition with not enough focus on mixed traffic conditions [45], [46].

In general, microsimulation practices can provide meaningful insight into traffic behavior, but the integrity of the outcomes is highly sensitive to the adequacy of the calibration of the base models used to ensure closeness to the expected real-life conditions. In some sense, the traffic model can describe traffic behavior qualitatively, whereas the calibration of the model tunes the characteristics quantitatively. There are typically two basic methods of trajectory-based optimization processes. In the global-fit approach, the position and speed of the follower are only used as input in the first time step, and the trajectory is updated serially at each later time step, which forms a time-continuous and sequential model of the acceleration function. The complete trajectory data is then compared with the simulated trajectory. This approach is usually non-linear, non-convex, and represents the more difficult optimization task. In the local-fit approach, the position and speed of the follower are input at each time step to compute the car-following behavior at the next time-step only, which translates into a discrete and time-continuous calibration task. Although this approach is less realistic and flexible, it requires significantly less computational power. Many mathematical formulations have been employed for microscopic model calibration using trajectory data, such as trial-and-error Iterative Adjustments (IA) algorithms [47], Genetic Algorithms solution [48], Simultaneous Perturbation Stochastic Approximation (SPSA) algorithms [49], [50] or Memetic Algorithms [51]. Li et al. [52] perform a rigorous comparison of many types of non-linear optimization processes and develop their own by combining a Lipschitzian search algorithm with a local search method. It was reported that the new model finds the global minimum solution 98 % of the time. These methods have been widely implemented

for the calibration of microscopic models of HDVs, but the lack of data regarding automated driving has hindered the calibration of the CAV car-following behavior. It is only recently that companies have started testing their prototypes in large-scale scenarios, hence enabling data to be collected and compiled for the research community. Large-scale testing with conventional vehicles has provided valuable information on how a CAV and an HDV may interact with each other. For example, the Waymo Open dataset contains high-resolution sensor data collected by Waymo automated vehicles across several cities in the US and in a wide range of mixed traffic situations.

As demonstrated above, there are several research gaps on mixed traffic flow, primarily due to (1) a lack of complexity in terms of the traffic compositions, (2) the oversimplistic one-dimensional analysis of non-critical situations, and (3) a lack of optimization to facilitate accurate results. Therefore, this paper seeks to develop a mixed traffic model that describes inter-vehicular interactions of CAVs and HDVs and extends the traffic model to a two-dimensional analysis by enabling lane-changing maneuvers. The traffic model can then be optimized with data from the Waymo Open dataset to ensure an accurate description of each interaction, hence enabling a more accurate evaluation of mixed traffic performance.

III. METHODOLOGY

To gain a more profound understanding of mixed traffic dynamics, this paper will investigate mixed traffic comprising HDVs and CAVs in a multilane freeway with an attached on-ramp acting as a disturbance to the free-flowing traffic. The traffic performance of the study environment is investigated in terms of travel times, throughput, and stability from 0 % to 100 % CAV penetration. The proposed mixed traffic model conveys the expected inter-vehicular interactions through model parameters that have been optimized with real-life data from the Waymo Open dataset.

A. CAR-FOLLOWING MODEL

The car-following model describes the longitudinal behavior of a vehicle with respect to a leader in the same lane, typically by prescribing an acceleration component. Gipps [53] developed the first popular car-following model to analyze traffic performance, after which several others followed [54]. Unfortunately, many of these are obsolete for CAVs because of the inherently different control mechanisms of these automated vehicles [55].

This study uses the Intelligent Driver Model (IDM) as the base longitudinal model as it is easily adaptable to different vehicle types, produces realistic acceleration profiles, allows for rapid simulation, and may be calibrated from empirical data [56]. In the IDM model equations, the acceleration is assumed to be a continuous function of the following vehicle's velocity, the distance gap, and the approaching rate (relative velocity), as defined by (1). This expression is "an interpolation of the tendency to maintain a nominal acceleration in normal conditions (denoted by 'a'), and the tendency to brake with deceleration (denoted by 'b') when the follower is too close to its leader" [57](p. 6). Moreover, the desired minimum gap dynamically varies with the velocity and approaching rate as defined by (2).

$$\ddot{x}_{n+1(t)} = \left[1 - \left(\frac{\dot{x}_{n+1(t)}}{\dot{x}_0}\right)^{\delta} - \left(\frac{S^*\left\{\dot{x}_{n+1(t),\Delta\dot{x}_{n+1(t)}}\right\}}{S_{n+1(t)}}\right)^2\right] \tag{1}$$

$$S^*\left\{\dot{x}_{n+1(t),\Delta\dot{x}_{n+1(t)}}\right\} = S_0 + \dot{x}_{n+1(t)}.T + \frac{\left\{\dot{x}_{n+1(t).\Delta\dot{x}_{n+1(t)}}\right\}}{2\sqrt{ab}} \tag{2}$$

where $\dot{x}_{n+1(t)}, \ddot{x}_{n+1(t)}$ are the velocity and acceleration of the follower car; $S^*\left\{\dot{x}_{n+1(t),\Delta\dot{x}_{n+1(t)}}\right\}$ is the desired gap between two adjacent cars; $\Delta\dot{x}_{n+1(t)}$ is the velocity difference between the leader (n) and the following (n+1) car; $\dot{x}_0$ is the free flow velocity; T is the safe time headway between two adjacent cars; a is the acceleration in normal traffic scenario; b is the comfortable braking deceleration in normal traffic scenario; S_0 is the minimum bumper to a bumper distance of two adjacent cars; $S_n = x_{n-1} - x_n - l_c$, where l_c is the length of the leader car, and δ is the constant acceleration exponent.

B. LANE-CHANGING MODEL

In this study, the lane-changing model describes the binary decision process of a lane change. Although lane-changing models have been much less explored than car-following, considerable effort has been made to describe lane-changing maneuvers [58], [59], [60], [61].

This study uses the Minimalizing Overall Braking Induced by Lane-change (MOBIL) model due to its compact formulation, which significantly reduces the complexity of microsimulation. Further, since MOBIL is based on IDM, the properties of the car-following model are transferred to the lane-changing model; therefore, the inter-vehicular interactions modelled in the IDM are applicable to MOBIL. The model is time-continuous and formulates the binary checks to be performed before a lane change is performed. In the MOBIL model, a lane change is performed when (a) a safety criterion is met by limiting the maximum deceleration rate to a pre-defined limit, and (b) an incentive criterion is met by ensuring that a lane change maneuver would improve the traffic conditions for the relevant road users. The MOBIL safety and incentive criteria are based on the car-following accelerations derived from the underlying car-following algorithm (IDM) and are defined by (3), and (4), respectively. We use a symmetrical lane-changing directive in this paper, where a vehicle is not restricted to a lane change in any direction.

$$\tilde{a} \geq -b_{safe} \tag{3}$$

$$(\tilde{a}_c - a_c) + p.(\tilde{a}_n - a_n + \tilde{a}_o - a_o) \geq \Delta a_{th} \tag{4}$$

where $\tilde{a}_n$ is the deceleration of the successor on the target lane; b_{safe} is a safe deceleration limit, $\tilde{a}_c$, $\tilde{a}_n$, and $\tilde{a}_o$ are the

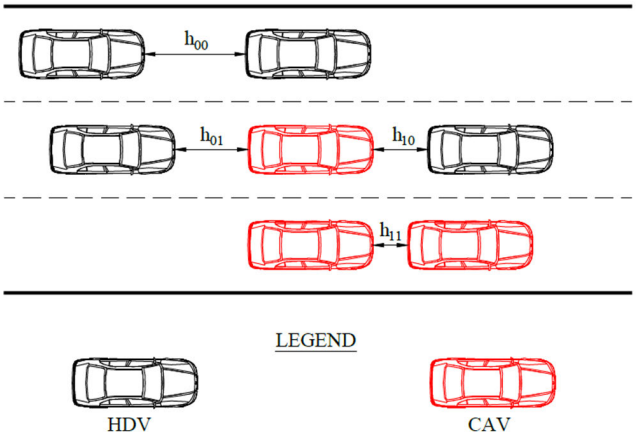

FIGURE 1. Overview of the four configurations.

new decelerations of the lane-changing vehicle, the succeeding vehicles on the target and the current lane respectively; a_c, a_n and a_o current decelerations of the lane-changing vehicle, the succeeding vehicles on the target and the current lane respectively; and p is the politeness factor; Δa_{th} is the lane change threshold. Quantities with a tilde refer to a new configuration after a lane change.

C. PROPOSED MICROSCOPIC TRAFFIC MODEL

To develop the new microscopic traffic model that describes inter-vehicular interactions, we must first delineate their different driving and communication mechanisms. Firstly, CAVs are fully connected to each other via V2V connectivity and can exchange information with each other instantaneously – this leads to deterministic, low-variance acceleration profiles and speed distributions. Moreover, a CAV can identify the vehicle types of all vehicles in its immediate surroundings. On the other hand, HDVs have stochastic behavior, and cannot identify the vehicle types of surrounding CAVs and HDVs.

In the car-following behavior, the IDM algorithm (2) is made to accommodate each of the four possible interactions by modifying the time headway parameter value. Fig. 1 denotes the time headway of each interaction as follows: (1) time headway between a following CAV and leading CAV, denoted by h_{11}; (2) time headway between a following CAV and leading HDV, denoted by h_{10}; (3) time headway between a following HDV and a leading CAV, denoted by h_{01}; and (4) time headway between a following HDV and leading HDV, denoted by h_{00}. The initial setting of the IDM time headway parameter will form the basic definition of the car-following behavior of each interaction before optimization. Eventually, the IDM model parameters will be optimized for each interaction. The following assumptions were employed in the initial time headway settings:

- CAV-CAV – The time headway between two CAVs (or the intra-platoon headway) is the lowest of the four possible interactions. This is due to the advantage that automation and connectivity offers. In the current HDV-dominated environment, it is less likely for a CAV to encounter another CAV, hence making modeling the interaction difficult.
  $h_{11} = \min\{h_{11}, h_{10}, h_{01}, h_{00}\}$
- CAV-HDV – When a CAV follows an HDV, there is a degradation of the longitudinal control from CACC to ACC due to a loss of connectivity, and therefore, communication. Therefore, the time headway is higher than when a CAV follows another CAV.
  $h_{10} > h_{11}$
- HDV-CAV – Given the lack of conclusive behavioral data on HDVs being able to differentiate between a CAV and an HDV, we employ the principle that an HDV cannot differentiate between a leading CAV and HDV, and thus, treats them equally.
  $h_{01} = h_{00}$
- HDV-HDV – This interaction has been thoroughly analyzed and we assume that it constitutes the largest time headway value.
  $h_{00} = \max\{h_{11}, h_{10}, h_{01}, h_{00}\}$

A typical lane change is depicted in Fig. 2, where N_S and N_L respectively refer to the succeeding and leading vehicles on the target (new) lane, O_S and O_L respectively refer to the succeeding and leading vehicles on the current (old) lane, and V_C refers to the lane-changer. A successful lane change will involve the following behavior during the relaxation stage.

- A large gap is created between O_S and O_L, allowing O_S to adopt a larger acceleration to close the distance gap.
- The lane change creates a disturbance on N_S in the target lane. N_s is forced to decelerate to avoid a collision. Note that a lane change does not occur if the deceleration of N_S is unsafe with respect to (3).
- After a lane change, V_C will follow N_L(instead of O_L) and will adjust its acceleration based on this new interaction. Similarly, N_S will follow V_C and will adjusts its acceleration accordingly.

When a vehicle changes lanes, the traffic configuration, and therefore, the associated car-following interactions change. As a result, the properties of the inter-vehicular car-following interactions are transferred to the lane-changing model. The following steps represent the simulation procedure to implement a lane change.

Step 1 – Gather information about the current traffic configuration. ($t = t_0$)

To compute the possibility for a subject vehicle to initiate a lane change, environmental data (such as position and velocity) is collected at the current time, t_0, for the subject vehicle (V_C), the successors, and leaders on the target lane (N_S and N_L), and the current lane (O_S and O_L). We refer to the arrangement of the vehicles before a lane change as the initial configuration (Fig. 3). The data acquired allows for the computation of the initial IDM accelerations of V_C, N_S, and O_S, denoted by a_c, a_n snd a_o respectively in (4).

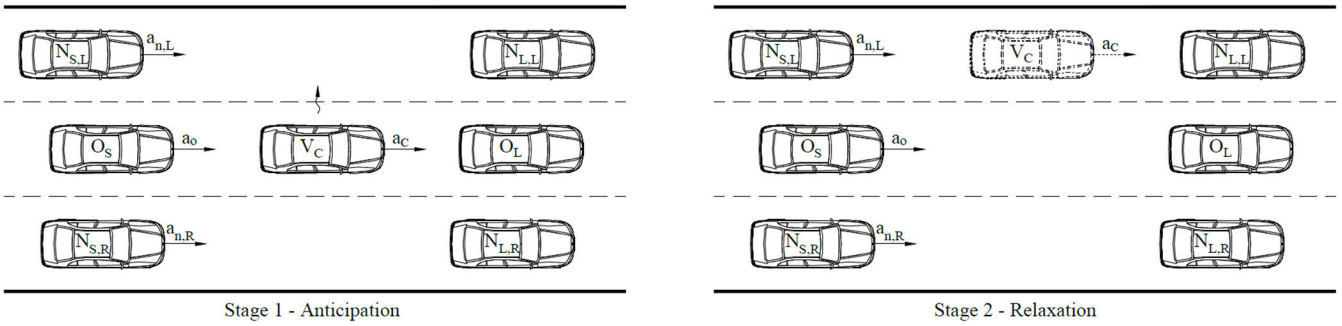

FIGURE 2. Typical lane change maneuver.

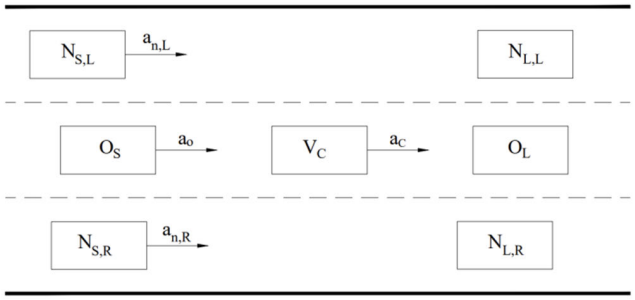

FIGURE 3. Initial configuration of a potential lane change at t_0.

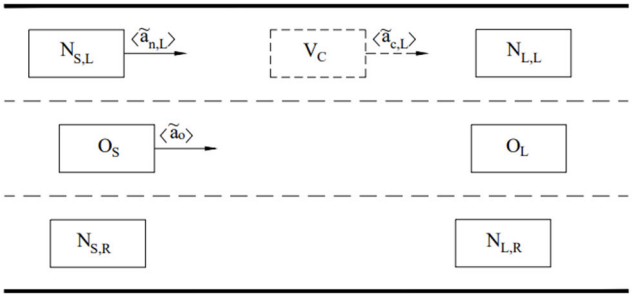

FIGURE 4. Virtual configuration of a lane change to the left.

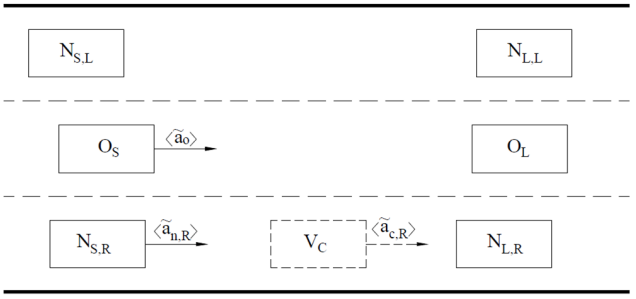

FIGURE 5. Virtual configuration of a lane change to the right.

The velocity and longitudinal position of the subject vehicle at the current time can be denoted by v_{t_0} and x_{t_0}, respectively.

Step 2 – Gather information about potential virtual traffic configurations. $(t = t_0)$

A virtual configuration must then be created for a lane change in each possible direction (Fig. 4 and Fig. 5) to represent the arrangement of vehicles after a potential lane change. A lane change to the left is denoted by the subscript "L", and a lane change to the right is denoted by the subscript "R". To create the virtual configuration, we assume that the vehicle has translated laterally to its target lane, either to the left or to the right. The potential IDM accelerations of the current vehicle, the old successor on the old lane, and the new successor on the target lane are then computed with (1) and (2). These are denoted by $\langle \tilde{a}_{c,L} \rangle$, $\langle \tilde{a}_o \rangle$, and $\langle \tilde{a}_{n,L} \rangle$ respectively, for a lane change to the left, and $\langle \tilde{a}_{c,R} \rangle$, $\langle \tilde{a}_o \rangle$, and $\langle \tilde{a}_{n,R} \rangle$ respectively for a lane change to the right. The velocity and longitudinal position of the subject vehicle under the virtual configurations are v_{t_0} and x_{t_0} respectively, but the subject vehicle is assumed to be on the target lane.

Step 3 – Check the MOBIL criteria of virtual configurations $(t = t_0)$

Once the IDM accelerations of V_C, N_S, and O_S are known in the initial configuration (before the lane change) and in the virtual configuration (after a potential lane change), the MOBIL criteria (3) and (4) must be checked. We highlight that if MOBIL finds that a lane change is possible in both directions, the subject vehicle will perform the lane change in the direction that offers the highest benefits. This represents the direction of the lane change which allows for the involved vehicles to adopt the highest accelerations and can be calculated from (5).

Highest benefits

$$= max \left[\sum \left(\langle \tilde{a}_{cL} \rangle - a_c \right) + p \cdot \left(\langle \tilde{a}_{nL} \rangle - a_n \right), \sum \left(\langle \tilde{a}_{cR} \rangle - a_c \right) + p \cdot \left(\langle \tilde{a}_{nR} \rangle - a_n \right) \right] \quad (5)$$

Step 4 – Initiation of the lane change. $(t = t_0 + \Delta t)$

If the MOBIL criteria (3) and (4) are met, the simulation will initiate a lane change in the next time step, $t = t_0 + \Delta t$. This step represents the anticipation stage of the lane change.

If the MOBIL criteria are not met, the simulation will not initiate the lane change. Therefore, the initial traffic configuration is maintained until the next time step, when the simulation procedure is reset.

The velocity and the longitudinal position of the vehicles at the initiation time step ($t = t_0 + \Delta t$) may be obtained from (6) and (7), respectively.

$$v_{t_0+\Delta t} = v_{t_0} + a_c.\Delta t \tag{6}$$
$$x_{t_0+\Delta t} = x_{t_0} + v_{t_0}.\Delta t \tag{7}$$

Step 5 – Completion of the lane change. ($t = t_0 + t_{LC}$)

If the MOBIL criteria (3) and (4) are met, and the subject vehicle initiates a lane change in the next time step as described in Step 4, we assume that the lane change will be completed in time t_{LC}, where $t_{LC} \leq 3\ s$. The velocity and the longitudinal position of the vehicles after a successful lane change may be calculated from (8) and (9).

$$v_{t_0+t_{LC}} = v_{t_0} + a_c.t_{LC} \tag{8}$$
$$x_{t_0+t_{LC}} = x_{t_0} + v_{t_0}.t_{LC} \tag{9}$$

At this step, one of the virtual configurations will be adopted as the new traffic configuration (Fig. 6 and Fig. 7), and the virtual accelerations are set as the new accelerations. This is the relaxation stage of the lane change maneuver.

For a lane change to the left,

$$\tilde{a}_{n,L} = \langle \tilde{a}_{n,L} \rangle \tag{10}$$
$$\tilde{a}_{c,L} = \langle \tilde{a}_{c,L} \rangle \tag{11}$$
$$\tilde{a}_o = \langle \tilde{a}_o \rangle \tag{12}$$

For a lane change to the right,

$$\tilde{a}_{n,R} = \langle \tilde{a}_{n,L} \rangle \tag{13}$$
$$\tilde{a}_{c,R} = \langle \tilde{a}_{c,R} \rangle \tag{14}$$
$$\tilde{a}_o = \langle \tilde{a}_o \rangle \tag{15}$$

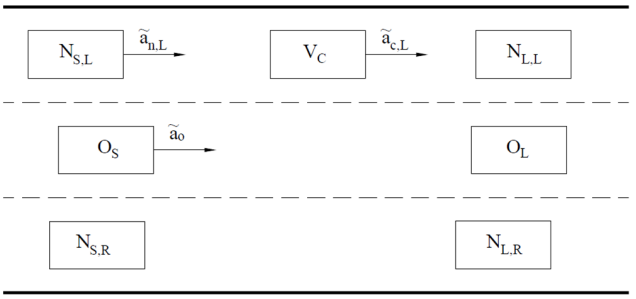

FIGURE 6. Adopted configuration of a successful lane change to the left.

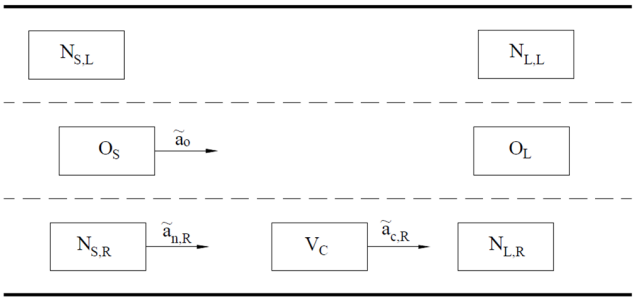

FIGURE 7. Adopted configuration of a successful lane change to the right.

TABLE 1. Vissim simulation settings.

Parameters	Value
Period	7200 s
Number of runs	10
Random Seed	50
Random Seed Increment	10
Number of Cores	1

D. SIMULATION ENVIRONMENT AND SETTINGS

The proposed two-dimensional microscopic model was tested in a simulation environment set out as a unidirectional three-lane freeway section, spanning a net distance of approximately 4.5 km. Buffer zones were provided at the start of the main section of the freeway to provide the spatial warm-up for vehicles entering the study environment, thereby facilitating accurate results. An on-ramp with an imposed speed limit of 70 km/hr was introduced at around 1.3 km along the freeway to act as an additional disturbance to the free-flowing traffic. An illustration of the study site is shown in Fig. 8, with 'X' denoting the distance along the freeway section.

The pipeline of the simulation can be summarized as:

- Vehicles are generated upstream of the road segment based on a specified traffic volume and vehicle composition (analogous to market penetration).
- Environmental data is collected for each driver at each timestep.
- The proposed microscopic traffic model is computed to control the behavior of the vehicle, following which the position of each vehicle is updated at each timestep.

Table 1 summarizes the simulation settings used in PTV Vissim. The vehicles are simulated for two hours, with results extracted from the 600 s mark onwards to provide a buffer period at the start of the simulation to allow for the traffic flow to stabilize and ensure accurate results. The simulations are run for a traffic volume assumed to be close to peak capacity, chosen as 3500 veh/hr on the main freeway and 1000 veh/hr on the on-ramp.

Table 2 summarizes the IDM-recommended parameter settings for HDVs and CAVs and is later optimized based on the four possible car-following interactions, with the initial headway settings for each interaction subsection in accordance with our previous assumptions listed in C.

This study deals with a minimalistic lane-changing MOBIL model, where the politeness factor is set to 1 and the lane-changing threshold is taken as 0.1 m/s^2 to limit unbeneficial stop-and-go jerks. Since this study deals with symmetrical lane-changing, the lane-changing bias is obsolete. The parameters used in the lane-changing model are summarized in Table 3.

E. OPTIMIZATION PROCEDURE

To ensure that our proposed model is accurately describing the expected real-world conditions, the model parameters

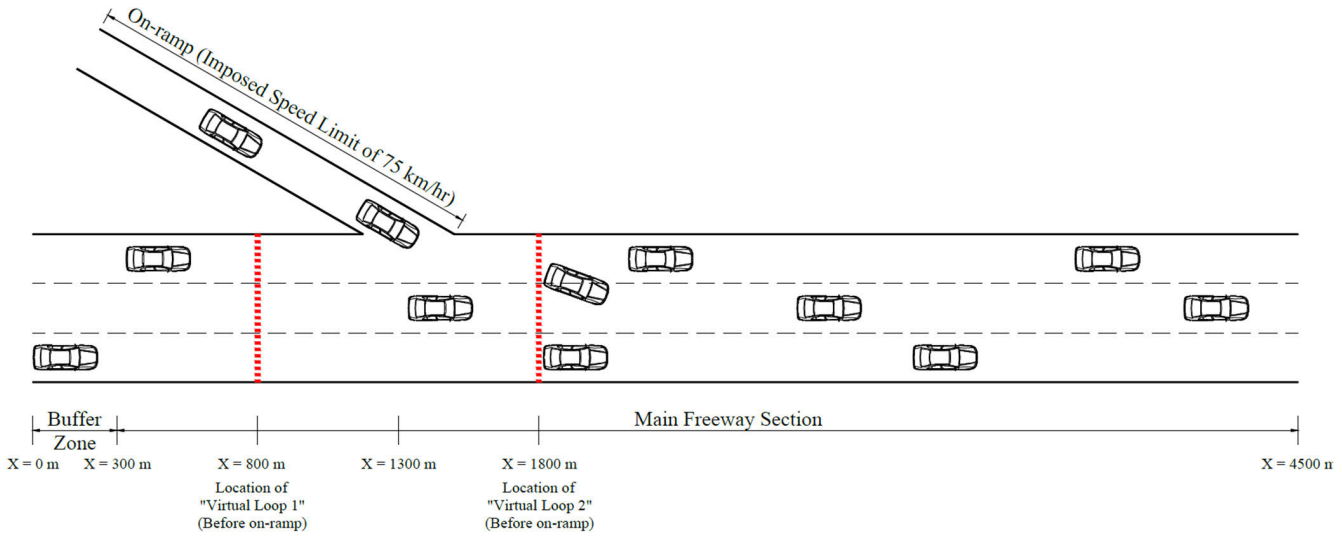

FIGURE 8. Overview of the study environment.

TABLE 2. IDM parameter settings.

Parameters	HDVs	CAVs
Free flow velocity, x_0 (Km/h)	100	100
Acceleration in normal traffic scenario, a (m/s^2)	1.4	1.5
Comfortable braking deceleration in normal traffic scenario, b (m/s^2)	2.0	3.0
Minimum bumper-to-bumper distance, S_0 (m)	2.0	2.0
Length of car, S_n (m)	4.5	4.5
Acceleration exponent, δ	4	4

TABLE 3. Mobil parameter settings.

Parameters	Value
Politeness Factor, p	1
Changing threshold, Δa_{th} (m/s^2)	0.1
Maximum Safe Deceleration, b_{safe} (m/s^2)	4.0
Bias for left/right lane, Δa_{bias} (m/s^2)	0

were calibrated using the Waymo Open dataset, which contains high-resolution sensor data collected by Waymo automated vehicles across several cities in the US, and in a wide range of mixed traffic scenarios. The dataset was initially created to help align efforts regarding automated vehicle driving, and contains trajectory data from 1000 segments, each with frames of data measured at 0.1 s intervals for 20 s. The curated and processed dataset by Hu et al. [62] was used in this paper.

The car-following parameters were optimized through a process proposed by Li et al. [52], who combine a global and local approach to the calibration task. In the first phase, a Lipschitzian global optimization is used known as DIRECT, named after its core process – DIviding RECTangles [63], [64]. During this phase, the first step is to transfer the initial solution space to a hyper-rectangle. Then, the center point of that hyper-rectangle is picked to evaluate the objective function and the hyper-rectangle is divided into smaller rectangles iteratively. By doing so, a set of potentially optimum subspaces are identified with a high probability of enclosing the global minimum. An overview of the process is given in Appendix B. Once a termination criterion is met, and a pre-set number of rectangle divisions have been made, the algorithm will then switch to a local search method known as the SQP (Sequential Quadratic Programming) local search method. The SQP algorithm is then applied to all the identified subspaces from the first phase to find a local minimum in each of them. A local search method is chosen in the second phase to accelerate the overall convergence time because the solution space is relatively flat around the global minimum. Therefore, the DIRECT+SQP algorithm has a high probability of finding the global minimum rapidly. For conciseness, we do not discuss these algorithms and their mathematical formulations further, but instead, re-direct interested readers to the available literature.

For the car-following optimization problem, the IDM parameter vector $\theta = [a, b, T]$ were constrained within a potential solution space with a lower bound $\theta_{min} = [1\ m/s^2, 1\ m/s^2, 1\ s]$ and an upper bound $\theta_{max} = [10\ m/s^2, 10\ m/s^2, 5\ s]$, such that $\theta_{min} \leq \theta \leq \theta_{max}$. An objective function of the Sum of Square Errors of gap was used in the optimization task, which is expressed as in (16). The SSE of gap is

TABLE 4. Optimized IDM parameter settings.

Parameters	HDV-HDV	HDV-CAV	CAV-CAV	CAV-HDV
Free flow velocity, x_0 (Km/h)	100	100	100	100
Acceleration in normal traffic scenario, a (m/s^2)	1.28	1.28	1.35	1.35
Comfortable braking deceleration in normal traffic scenario, b (m/s^2)	1	1	1.01	1.01
Minimum bumper to bumper distance, S_0 (m)	2.0	2.0	2.0	2.0
Time Headway, T (s)	1.7	1.7	0.6	1.35
Acceleration exponent, δ	4	4	4	4

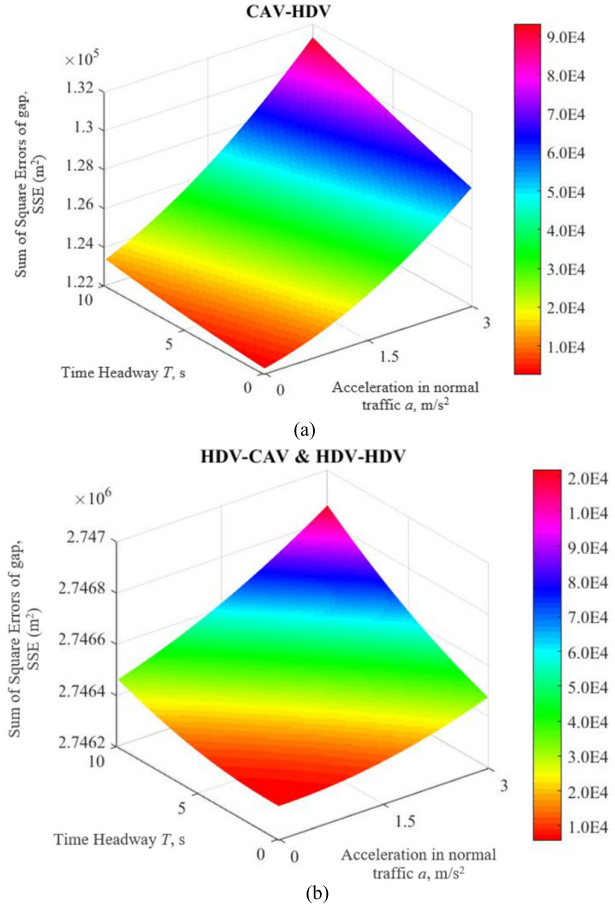

FIGURE 9. Fitting landscape with respect to parameters a and T for (a) CAV-HDV and (b) HDV-CAV & HDV-HDV.

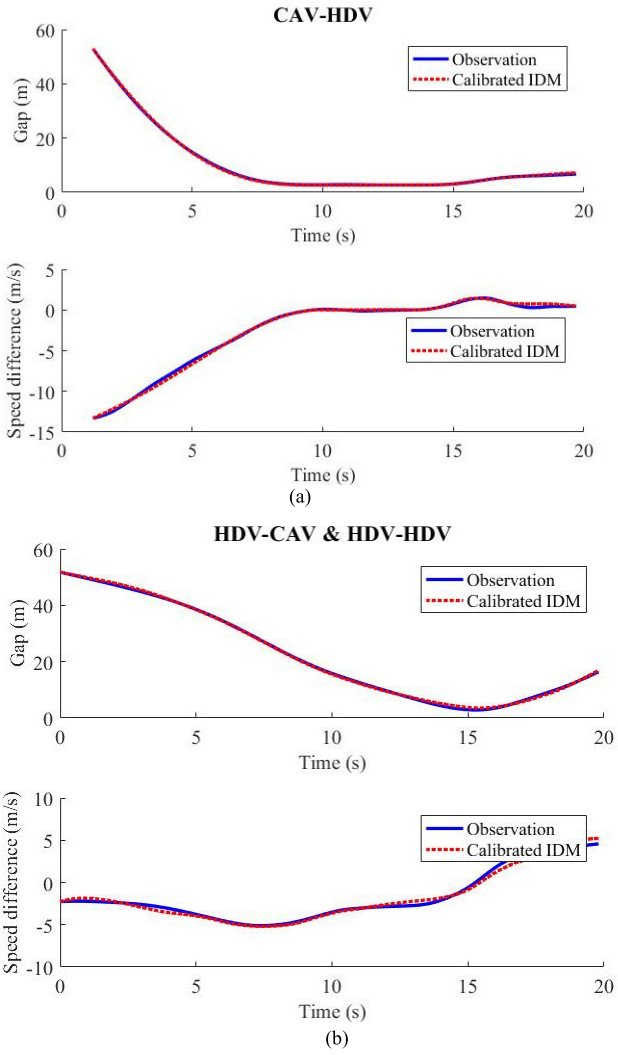

FIGURE 10. Comparison of the gap and speed difference for (a) CAV-HDV and (b) HDV-CAV & HDV-HDV.

thought to contain the most degrees of freedom and therefore, constitutes the most challenging calibration task. This is because platoon consistency may imply that cumulative differences between speed data may be zero in the long term. Conversely, no such restrictions apply to the distance gap. Moreover, speed or speed differences values are unsuitable for calibrating IDM time headway parameters [56].

$$\min_{\theta=\xi} f(\theta) = \sum_{i=1}^{N} \left[x_j(iT|\theta) - \widehat{x_j}(iT)\right]^2 \qquad (16)$$

where θ is the IDM parameter vector to be optimized; ξ is the solution space; i is the optimization iteration count; T is the time step of the optimization task; $x_j(iT|\theta)$ is the computed longitudinal position of the follower j at time iT; and $\widehat{x_j}(iT)$ is the observed longitudinal position of the follower j at time iT.

Three important assumptions are used in the calibration task, due to the limitations of data of the Waymo Open dataset:

- Since the number of automated vehicles available in the testing environment was quite low, the dataset does not contain data about the CAV-CAV interaction.

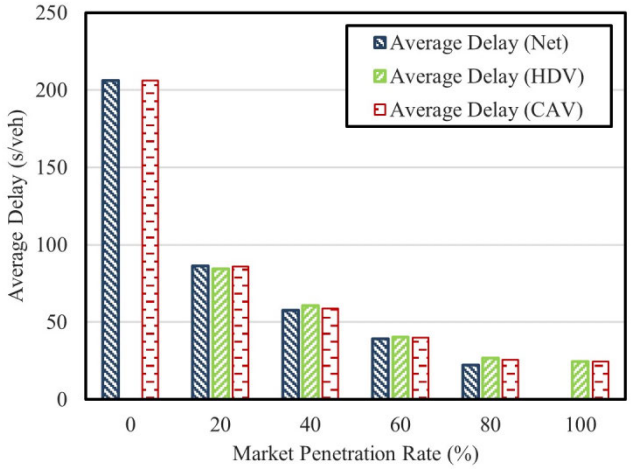

FIGURE 11. Average delay per vehicle at varying CAV penetration.

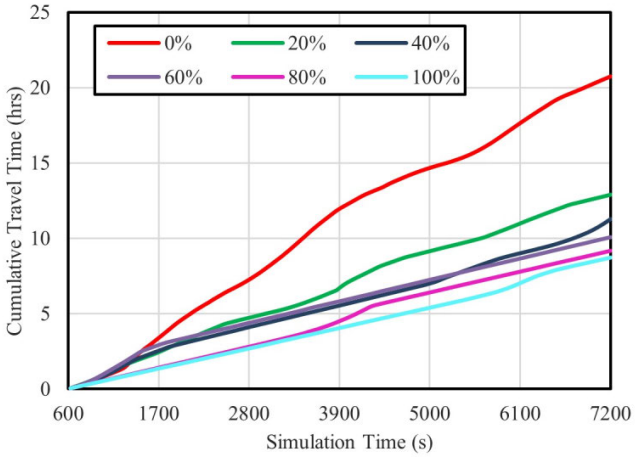

FIGURE 12. Cumulative travel time measured at 30-second intervals for varying CAV penetration.

However, the main advantage of this interaction comes from the improved communication behavior, which enables a CAV follower to acquire accurate information about speed differences and distance with its CAV leader. This would allow the following CAV to adopt a low time headway, which was chosen as 0.6 s [65], [66], [67].

- The data is incomplete for most trajectory sets concerning the main dynamic driving situations (accelerating, cruising, braking, and standstill) and does not contain standstill distances. Therefore, it was assumed that the standstill distance is 2.0 m irrespective of the car-following interaction.
- As discussed earlier, an HDV's car-following behavior is unchanged for a leading CAV and leading HDV. Therefore, the same set of model parameters apply for the HDV-CAV and HDV-HDV interactions.

IV. RESULTS & DISCUSSION

A. OPTIMIZATION RESULTS

The results of the optimization process are presented as follows. Fig. 9 shows the fitting landscape of the objective function around the global minimum solution, whereas Fig. 10 presents the data from the observed and calibrated models.

Referring to Fig. 9, the objective function was smooth and unimodal within the pre-defined boundary conditions, which is often impossible when calibrating incomplete single-vehicle trajectory data globally. However, by restricting the calibration only to parameters relevant to the Waymo Open dataset (and not calibrating standstill distances S_0), we escaped being stuck in a local secondary minimum or a fitting landscape with no unique minimum value. The optimized car-following parameters are summarized in Table 4.

B. NETWORK PERFORMANCE RESULTS

1) IMPACT ON TRAVEL TIME

Travel time and delay constitute the most significant measure of a user-oriented level of service. In the context of this paper, the experienced delays indicate the perceived traffic performance on an individual level, whereas the cumulative travel times are indicative of performance on a network level and are linked to the cost of travel. Delays and travel times were measured along the freeway section at 30-second intervals.

Fig. 11 shows the average relative delays (average delay per vehicle) at varying CAV penetration rates. Significant improvements occurred at very low CAV penetration, with the average relative delay decreasing by up to 100% from 0% to 20% CAVs. Overall, this trend was consistent with increasing CAV penetration, but the extent of the improvements decreased considerably. This observation suggests that the introduction of CAVs in conventional traffic would allow more vehicles to travel at their desired speeds, without being slowed down by the surrounding traffic.

Further, we observed that in mixed traffic, the average relative delay of a CAV was slightly higher than that of an HDV. This is because CAVs typically desire to travel at higher speeds, which they cannot reach due to the presence of slower-moving HDVs. Therefore, the *perceived* delays of CAVs were higher than HDVs. The findings suggest that as CAVs slowly infiltrate conventional traffic, the experienced level of service may decrease because CAV users may become accustomed to travel at higher speeds, and therefore, will *feel* slowed down by the presence of HDVs.

Fig. 12 shows the cumulative travel times at varying CAV penetration. The total travel time at 0% CAV penetration resulted in approximately 21 hours but amounted to only 9 hours at 100% CAV penetration. This amelioration in cumulative travel times was observed at low penetration rates and was consistent with increasing CAV penetration. This suggests that although users may *feel* slowed down as discussed above, the introduction of CAVs would also allow for shorter total travel times, hence resulting in a decrease in the cost of travel.

The instantaneous travel time in Fig. 13(a) shows multiple oscillations during the two-hour simulation at low CAV penetration (0% to 40%). These oscillations are representative

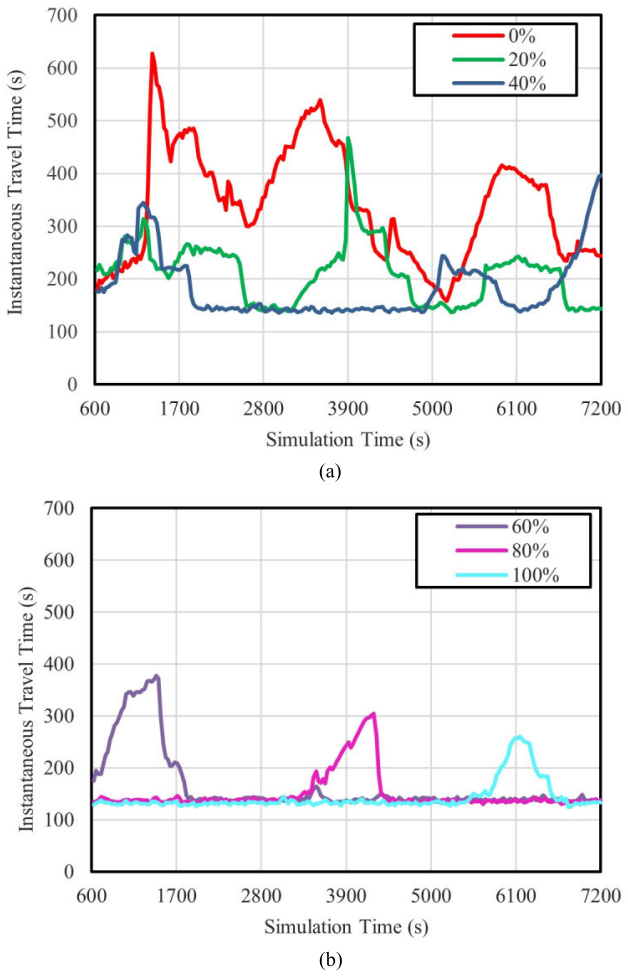

FIGURE 13. Instantaneous travel time measured at 30-second intervals for varying CAV penetration (a) 0, 20 & 40 % CAV penetration and (b) 60, 80 & 100 % CAV penetration.

of shockwaves that formed due to the disturbance caused by the on-ramp traffic and have an important role to play in the congestion levels across the freeway, contributing directly to an increase in delays. At 0% penetration, three major oscillations were observed. As the penetration of CAVs was increased, the amplitude and frequency of the oscillations decreased significantly, suggesting that CAVs were better able to cope with disturbance.

Moreover, it may be inferred from Fig. 13(b) that CAVs led to a temporal shift in the traffic breakdown represented by a peak in instantaneous travel time. For example, it was observed that the breakdown occurred at around 4000 s at 80% CAV penetration, and 6100 s at 100% CAV penetration. In other words, the traffic breakdown occurred 30 minutes later. In the real world, this improvement may be significant during peak-hour traffic. By delaying the formation of a traffic breakdown, traffic performance is preserved during the more critical middle phase of peak traffic. As the traffic volume decreases as we approach the end of peak hours, less vehicles are thereby affected by the traffic breakdown.

2) IMPACT ON THROUGHPUT

To imitate typical cross-sectional measurements of real-life data from inductor loop detectors, 'virtual detectors' were used in the simulations to analyze the traffic throughput, Q, and the mean harmonic velocity, v at 3-minute intervals. The hydrodynamic relationship $Q = \rho v$ was then used to estimate the traffic density, ρ. To better understand the impact of the merging traffic from the on-ramp (x = 1300 m), the virtual detectors were positioned 500 m before (x = 800 m) and 500 m after (x = 1800 m) the on-ramp, as depicted in the setup presented in Fig. 8. The data points collected from the virtual detectors were plotted in Fig. 14. The data points are labelled as ''Before'' and ''After'' for the virtual detectors upstream (x = 800 m) and downstream (x = 1300 m) of the bottleneck respectively.

At any CAV penetration, the data points upstream of the on-ramp showed linear behavior, hence depicting a free-flowing traffic regime. Conversely, the data points downstream of the on-ramp were widely scattered and random, indicative of a congested flow regime. This confirmed that the on-ramp traffic had a significant impact on the free-flowing traffic on the freeway and the creation of a bottleneck location near the on-ramp. However, CAVs were better able to negate the impacts of the on-ramp disturbance. As a result, the levels of congestion decreased at increasing CAV penetration, as indicated by the fact that the data points downstream of the on-ramp were less randomly scattered, falling increasingly within the linear region of the Q-ρ fundamental diagram.

In the same line, it was observed that the local capacity drops that occurred at the on-ramp decreased with increasing CAV penetration. For example, there was a decrease of approximately 15% in throughput identified at 0% CAV penetration. However, at 40% CAV penetration, there was a reduction of only 10% in throughput. This is thought to be because of the CAV's ability to adopt shorter time headways in the car-following behavior, thereby allowing them to 'absorb' the disturbance of the on-ramp traffic more easily. The dynamic improvement in local throughput that was observed at the on-ramp at high CAV penetration may be transferred to other types of similar bottleneck situations, such as in the event of a car breakdown.

3) IMPACT ON TRAFFIC STABILITY

Fig. 15 below shows the surface plot of the spatiotemporal traffic dynamics of the freeway with an attached on-ramp. The temporarily reduced speed area at the on-ramp bottleneck induced a reduction in local capacity and led to the formation of a shockwave. The average lane velocity of the freeway was plotted along the Z-axis of Fig. 15 to explain this phenomenon along the road during the simulation period.

The results demonstrated the formation of a backward forming shockwave that was caused by the merging on-ramp traffic. As a result, a queue was formed upstream of the on-ramp location. It was seen that with an increasing CAV penetration, the shockwave dissipated quicker. This

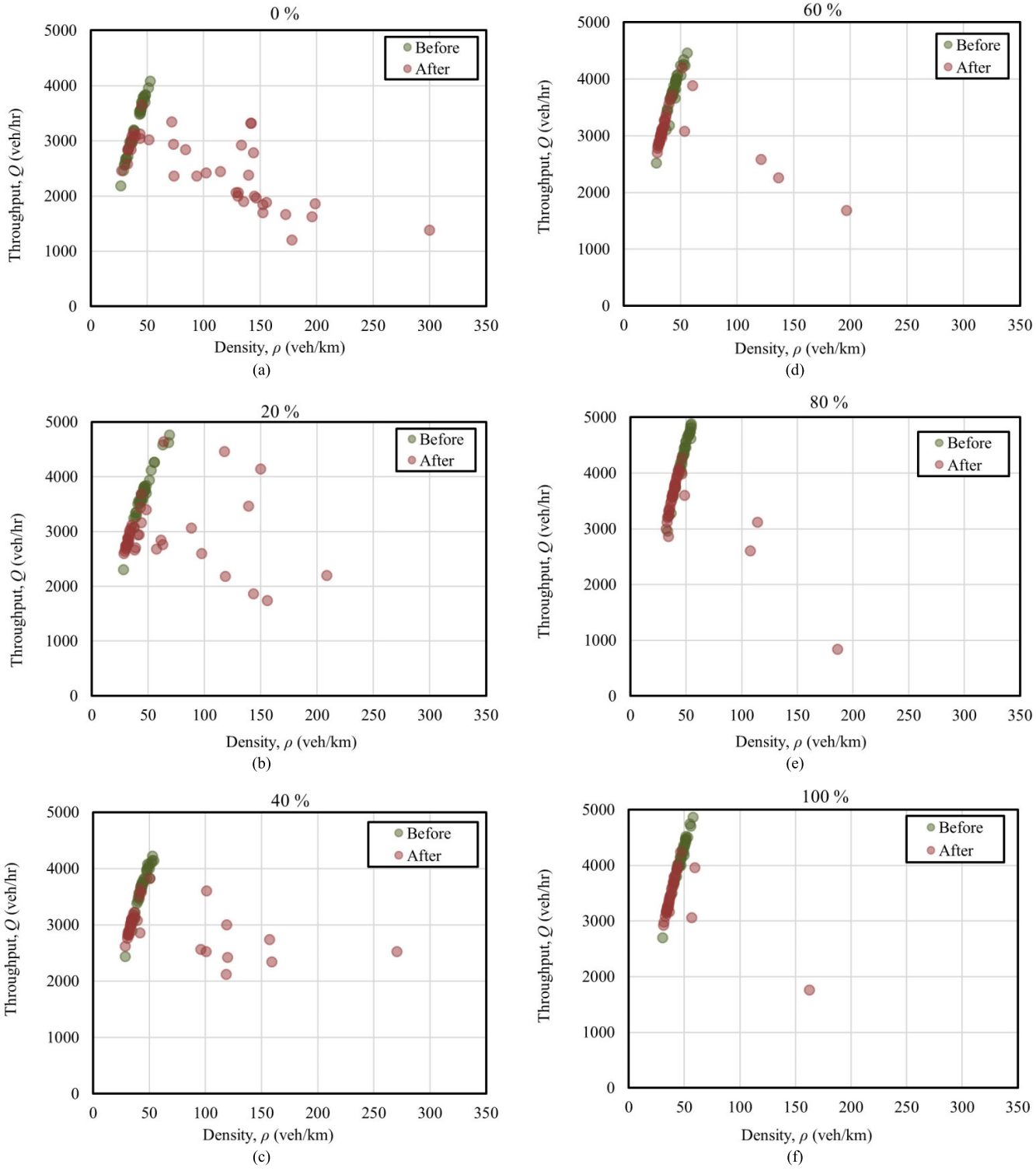

FIGURE 14. Flow-density data measured from 'virtual detectors' at 30-second intervals and averaged across three lanes. Data points are labelled 'Before' for the detector at 500 m before the on-ramp (x = 800 m) and 'After' for the detector at 500 m after the on-ramp (x = 1800m).

indicated that a CAV can easily adapt its speed when a traffic breakdown occurs. This led to smoother deceleration rates that have a lower impact on the succeeding vehicles, thereby facilitating the dissipation of the shockwave.

Further, it was observed that the congestion areas around the bottleneck were reduced at higher CAV penetration. This can be inferred from Fig. 15, which shows flat and deep oscillation peaks at low CAV penetration. With increasing

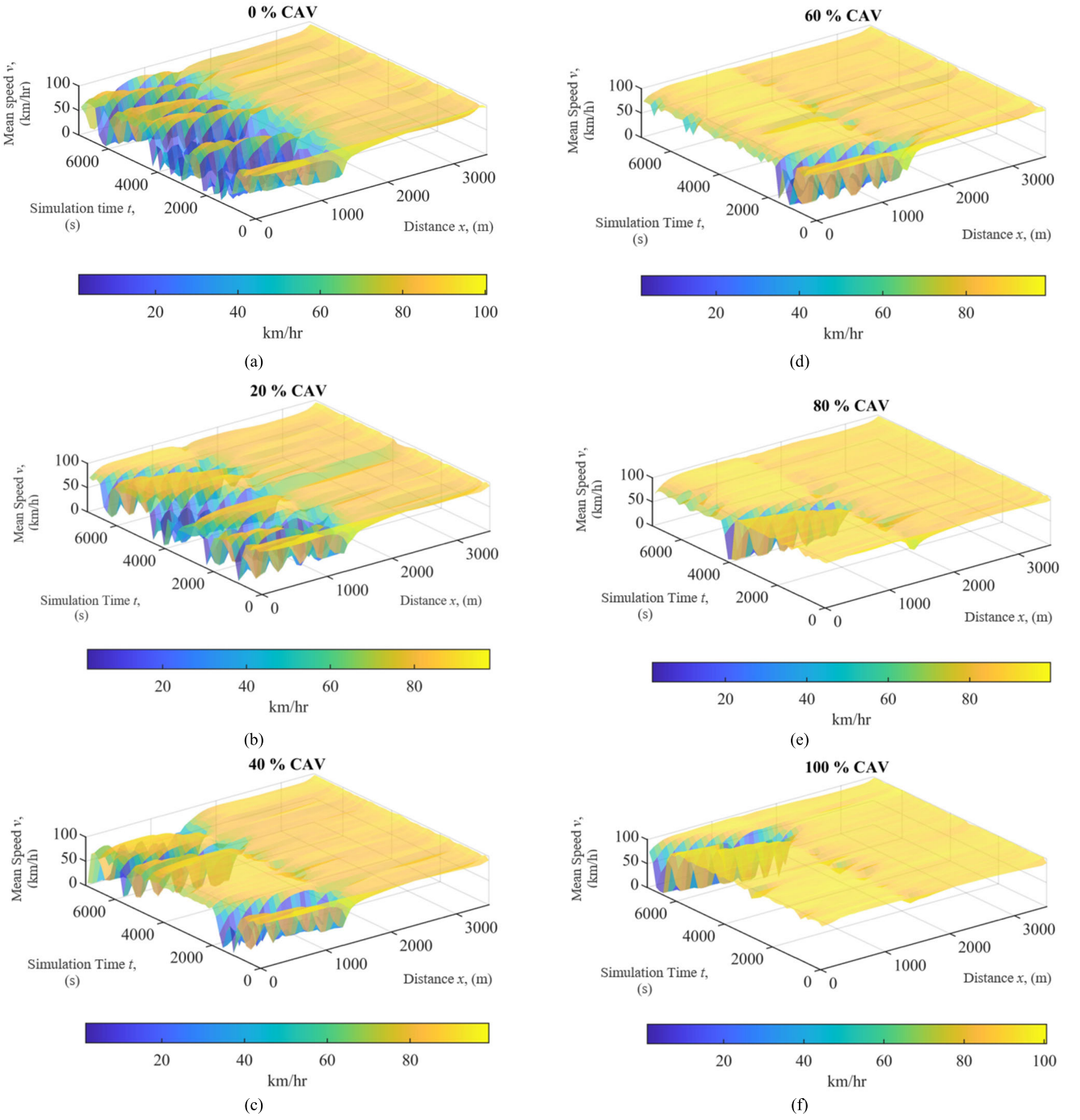

FIGURE 15. Spatiotemporal traffic dynamics along the freeway, measured at 10 m intervals in regular 30-second intervals.

CAV penetration, the peaks of oscillations are sharper and shallower, indicating that less areas of the road are congested with slower-moving vehicles.

As discussed in Section IV-A, Fig. 15 also shows that CAVs may delay the formation of shockwaves. In this study, the shockwave was not eliminated due to the high traffic volume of the disturbing on-ramp traffic, and its imposed speed limit. However, the presence of CAVs noticeably reduced traffic congestion and led to higher string stability.

V. CONCLUSION

This paper proposes a data-driven two-dimensional microscopic traffic model that considers the inter-vehicular interactions between HDVs and CAVs. By using a lane-changing model that is based on the car-following model, the inter-vehicular interactions of the car-following model are transferred to the lane-changing model. The four possible car-following interactions were optimized from trajectory data of the Waymo Open dataset and utilizing a combination

TABLE 5. List of notations used.

Notation	Meaning	Unit
$\dot{x}_{n+1}(t)$	Velocity of following car in car-following model	m/s
$\ddot{x}_{n+1}(t)$	Acceleration of following car in car-following model	m/s^2
$s^*\left(\ddot{x}_{n+1}(t), \Delta\dot{x}_{n+1}(t)\right)$	Desired gap between two adjacent cars in car-following model	m
$\Delta\dot{x}_{n+1}(t)$	Velocity difference between leader and follower in car-following model	m/s
$\dot{x}_0$	Free flow velocity	m/s
T	Safe time headway between two adjacent cars	s
a	Acceleration in normal traffic scenario	m/s^2
b	Comfortable braking deceleration in normal traffic scenario	m/s^2
s_0	Minimum bumper to bumper distance of two adjacent cars	m
s_n	Distance gap between two adjacent cars	m
l_c	Length of the leader car	m
δ	Constant acceleration exponent	m/s^2
b_{safe}	Safe deceleration limit in lane-changing model	m/s^2
$\tilde{a}_{c,left}$	New accelerations of the subject vehicle, after a lane change to the left	m/s^2
$\tilde{a}_{c,right}$	New accelerations of the subject vehicle, after a lane change to the right	m/s^2
$\tilde{a}_{n,left}$	New accelerations of the succeeding vehicle on the target lane, after a lane change to the left	m/s^2
$\tilde{a}_{n,right}$	New accelerations of the succeeding vehicle on the target lane, after a lane change to the right	m/s^2
$\tilde{a}_o$	New accelerations of the succeeding vehicle on the current lane, after a lane change	m/s^2
a_c	Old acceleration of the subject vehicle, before a lane change	m/s^2
$a_{n,left}$	Old acceleration of the succeeding vehicle on the target lane to the left, before a lane change	m/s^2
$a_{n,right}$	Old acceleration of the succeeding vehicle on the target lane to the right, before a lane change	m/s^2
a_o	Old acceleration of the succeeding vehicle on the current lane, before a lane change	m/s^2
v_c	Velocity of the subject vehicle	m/s
$\tilde{v}_{lead}$	Velocity of the leader vehicle on the target lane of a lane change	m/s
v_{crit}	Typical Velocity in congested traffic	m/s
p	Politeness factor in lane-changing model	-
Δa_{th}	Lane-changing threshold	m/s^2
Δa_{bias}	Lane-changing constant bias	m/s^2
$N_{s,left}$	New successor on target lane, after a lane change to the left	-
$N_{s,right}$	New successor on target lane, after a lane change to the right	-
$N_{L,left}$	New leader on target lane, after a lane change to the left	-

of a Lipschitzian Optimization algorithm and a local search method.

The optimized model was then tested on a three-lane freeway with an attached on-ramp to investigate mixed traffic performance at varying CAV penetration. At higher CAV penetration, the results suggested a deterioration in perceived experienced delays on an individual level, but a significant improvement in total travel times, and therefore the cost of travel, on a network level. Further, CAVs were better at dealing with disturbance from the on-ramp traffic, and therefore, they were able to maintain a stable free-flowing traffic. In the same line, the local capacity drop at the on-ramp decreased significantly at higher CAV penetration. It was also noted that the presence of CAVs led to a temporal shift in the traffic breakdown, hence delaying the formation of a shockwave. This finding is thought to be significant during peak hour traffic and would likely cause less vehicles to be negatively affected by the traffic breakdown.

Future research should evaluate the use of this model in other critical traffic situations to validate the improvements that this paper suggests at higher CAV market penetration. Further work should also aim to optimize performance in mixed traffic scenarios; this can be possible with dedicated automated driving lanes or platooning mechanisms. This would assist in formulating a framework that can be used to facilitate the imminent deployment of CAVs.

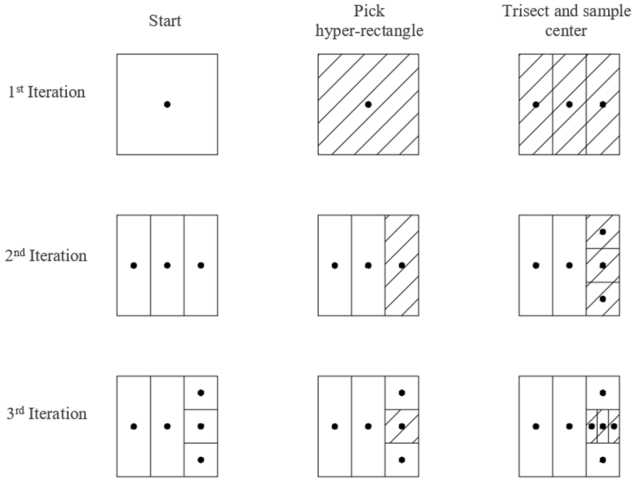

FIGURE 16. Overview of the search and dividing process of the DiRECT algorithm proposed by Jones [63] after three iterations. The hatched rectangles represent the subspaces of interest at each iteration.

APPENDIX A
OVERVIEW OF DIRECT ALGORITHM

See Figure 16.

APPENDIX B
LIST OF NOTATIONS

See Table 5.

ACKNOWLEDGMENT

The authors thank the Waymo team for sharing their open-access dataset and Hu et al. [62] for curating the data and providing insightful comments.

REFERENCES

[1] R. Lanctot, "Accelerating the future: The economic impact of the emerging passenger economy," *Strategy Anal.*, vol. 5, pp. 1–30, Jun. 2017.

[2] J. Zhou and F. Zhu, "Modeling the fundamental diagram of mixed human-driven and connected automated vehicles," *Transp. Res. C, Emerg. Technol.*, vol. 115, Jun. 2020, Art. no. 102614, doi: 10.1016/j.trc.2020.102614.

[3] Z. Li, X. Huang, J. Wang, and T. Mu, "Lane change behavior research based on NGSIM vehicle trajectory data," in *Proc. Chinese Control Decis. Conf. (CCDC)*, Hefei, China, 2020, pp. 1865–1870, doi: 10.1109/CCDC49329.2020.9164679.

[4] Y. Fang, Z. Shi, and J. Cao, "Calibration of an interrupted traffic flow system using NGSIM trajectory data sets," in *Proc. 11th World Congr. Intell. Control Automat.*, Shenyang, China, 2014, pp. 4887–4892, doi: 10.1109/WCICA.2014.7053542.

[5] W. Liu, Q. Dong, P. Wang, G. Yang, L. Meng, Y. Song, Y. Shi, and Y. Xue, "A survey on autonomous driving datasets," in *Proc. 8th Int. Conf. Dependable Syst. Their Appl. (DSA)*, Yinchuan, China, 2021, pp. 399–407, doi: 10.1109/DSA52907.2021.00060.

[6] P. A. Ioannou and M. Stefanovic, "Evaluation of ACC vehicles in mixed traffic: Lane change effects and sensitivity analysis," *IEEE Trans. Intell. Transp. Syst.*, vol. 6, no. 1, pp. 79–89, Mar. 2005, doi: 10.1109/TITS.2005.844226.

[7] H. Liu, X. D. Kan, S. E. Shladover, X.-Y. Lu, and R. E. Ferlis, "Modeling impacts of cooperative adaptive cruise control on mixed traffic flow in multi-lane freeway facilities," *Transp. Res. C, Emerg. Technol.*, vol. 95, pp. 261–279, Oct. 2018, doi: 10.1016/j.trc.2018.07.027.

[8] S. Ahn and M. Cassidy, "Freeway traffic oscillations and vehicle lane-change maneuvers," in *Proc. 17th Int. Symp. Transp. Traffic Theory*, London, U.K., 2007, pp. 1–23.

[9] R. V. Rabsatt and M. Gerla, "Multi-lane cooperative shock wave mitigation," in *Proc. 16th Annu. Medit. Ad Hoc Netw. Workshop (Med-Hoc-Net)*, Jun. 2017, pp. 1–7, doi: 10.1109/MedHocNet.2017.8001648.

[10] J. Nie, J. Zhang, W. Ding, X. Wan, X. Chen, and B. Ran, "Decentralized cooperative lane-changing decision-making for connected autonomous vehicles," *IEEE Access*, vol. 4, pp. 9413–9420, 2016, doi: 10.1109/ACCESS.2017.2649567.

[11] F. A. Mullakkal-Babu, M. Wang, B. van Arem, and R. Happee, "Empirics and models of fragmented lane changes," *IEEE Open J. Intell. Transp. Syst.*, vol. 1, pp. 187–200, 2020, doi: 10.1109/OJITS.2020.3029056.

[12] D. Yang, L. Zhu, Y. Liu, D. Wu, and B. Ran, "A novel car-following control model combining machine learning and kinematics models for automated vehicles," *IEEE Trans. Intell. Transp. Syst.*, vol. 20, no. 6, pp. 1991–2000, Jun. 2019, doi: 10.1109/TITS.2018.2854827.

[13] K. Chen, P. Liu, Z. Li, Y. Wang, and Y. Lu, "Modeling anticipation and relaxation of lane changing behavior using deep learning," *Transp. Res. Rec., J. Transp. Res. Board*, vol. 2675, no. 12, pp. 186–200, Dec. 2021, doi: 10.1177/03611981211028624.

[14] L. Saleh, P. Chevrel, F. Mars, J.-F. Lafay, and F. Claveau, "Human-like cybernetic driver model for lane keeping," *IFAC Proc. Volumes*, vol. 44, no. 1, pp. 4368–4373, Jan. 2011, doi: 10.3182/20110828-6-IT-1002.02349.

[15] M. Brackstone, B. Waterson, and M. McDonald, "Determinants of following headway in congested traffic," *Transp. Res. F, Traffic Psychol. Behaviour*, vol. 12, no. 2, pp. 131–142, Mar. 2009, doi: 10.1016/j.trf.2008.09.003.

[16] T. Litman, "Autonomous vehicle implementation predictions implications for transport planning," Victoria Transport Institute, Victoria, BC, Canada, Tech. Rep., 2022.

[17] X. Di and R. Shi, "A survey on autonomous vehicle control in the era of mixed-autonomy: From physics-base to AI-guided driving policy learning," *Transp. Res. C, Emerg. Technol.*, vol. 125, pp. 1–50, Apr. 2021.

[18] J. Rios-Torres and A. A. Malikopoulos, "A survey on the coordination of connected and automated vehicles at intersections and merging at highway on-ramps," *IEEE Trans. Intell. Transp. Syst.*, vol. 18, no. 5, pp. 1066–1077, May 2017, doi: 10.1109/TITS.2016.2600504.

[19] P. Sukkenik, *Micro-Simulation Guide for Automated Vehicles*, document D2.11, PTV Group, Karlsruhe, Germany, CoExist, May 2019.

[20] B. Khondaker and L. Kattan, "Variable speed limit: A microscopic analysis in a connected vehicle environment," *Transp. Res. C, Emerg. Technol.*, vol. 58, pp. 146–159, Sep. 2015, doi: 10.1016/j.trc.2015.07.014.

[21] I. Mavromatis, A. Tassi, R. J. Piechocki, and M. Sooriyabandara, "On urban traffic flow benefits of connected and automated vehicles," in *Proc. IEEE 91st Veh. Technol. Conf. (VTC-Spring)*, Antwerp, Belgium, May 2020, pp. 1–7, doi: 10.1109/VTC2020-Spring48590.2020.9128758.

[22] *Research on the Impacts of Connected and Autonomous Vehicles (CAVs) on Traffic Flow*, Department for Transport, Atkins, Epsom, U.K., May 2016.

[23] Z. Yao, Q. Gu, Y. Jiang, and B. Ran, "Fundamental diagram and stability of mixed traffic flow considering platoon size and intensity of connected automated vehicles," *Phys. A, Stat. Mech. Appl.*, vol. 604, Oct. 2022, Art. no. 127857, doi: 10.1016/j.physa.2022.127857.

[24] Z. Yao, Y. Wu, Y. Jiang, and B. Ran, "Modeling the fundamental diagram of mixed traffic flow with dedicated lanes for connected automated vehicles," *IEEE Trans. Intell. Transp. Syst.*, vol. 24, no. 6, pp. 6517–6529, Jun. 2023, doi: 10.1109/TITS.2022.3219836.

[25] M. Gouy, K. Wiedemann, A. Stevens, G. Brunett, and N. Reed, "Driving next to automated vehicle platoons: How do short time headways influence non-platoon drivers' longitudinal control?" *Transp. Res. F, Traffic Psychol. Behaviour*, vol. 27, pp. 264–273, Nov. 2014, doi: 10.1016/j.trf.2014.03.003.

[26] M. Gouy, "Behavioral adaptation of drivers of unequipped vehicles to short time headways observed in a vehicle platoon," Ph.D. Dissertations, Transp. Res. Lab.-Affiliated Res. Centre Open Univ., U.K., 2013.

[27] S. van de Hoef, K. H. Johansson, and D. V. Dimarogonas, "Fuel-efficient en route formation of truck platoons," *IEEE Trans. Intell. Transp. Syst.*, vol. 19, no. 1, pp. 102–112, Jan. 2018, doi: 10.1109/TITS.2017.2700021.

[28] Z. Wang, G. Wu, P. Hao, K. Boriboonsomsin, and M. Barth, "Developing a platoon-wide eco-cooperative adaptive cruise control (CACC) system," in *Proc. IEEE Intell. Vehicles Symp. (IV)*, Jun. 2017, pp. 1256–1261, doi: 10.1109/IVS.2017.7995884.

[29] V. Turri, B. Besselink, and K. H. Johansson, "Cooperative look-ahead control for fuel-efficient and safe heavy-duty vehicle platooning," *IEEE Trans. Control Syst. Technol.*, vol. 25, no. 1, pp. 12–28, Jan. 2017, doi: 10.1109/TCST.2016.2542044.

[30] Z. Wang, Y. Bian, S. E. Shladover, G. Wu, S. E. Li, and M. J. Barth, "A survey on cooperative longitudinal motion control of multiple connected and automated vehicles," *IEEE Intell. Transp. Syst. Mag.*, vol. 12, no. 1, pp. 4–24, Spring. 2020, doi: 10.1109/MITS.2019.2953562.

[31] Y. Li, C. Tang, S. Peeta, and Y. Wang, "Nonlinear consensus-based connected vehicle platoon control incorporating car-following interactions and heterogeneous time delays," *IEEE Trans. Intell. Transp. Syst.*, vol. 20, no. 6, pp. 2209–2219, Jun. 2019, doi: 10.1109/TITS.2018.2865546.

[32] C. Wu, E. Vinitsky, and A. M. Bayen, "Emergent behaviors in mixed-autonomy traffic," in *Proc. 1st Conf. Robot. Learn.*, Oct. 2017, pp. 1–10.

[33] N. Motamedidehkordi, T. Benz, and M. Margreiter, "Effects of connected highly automated vehicles on the propagation of congested patterns on freeways," in *Proc. 95th Annual Meeting Transp. Res. Board*, Washington, DC, USA, Jan. 2016, pp. 1–16, doi: 10.13140/RG.2.1.3084.9689.

[34] A. Maarafi and W. Virginia, "The impact of autonomous vehicles on freeway throughput," Ph.D. Dissertation, Dept. Civil Env. Eng., Univ. West Virginia, Morgantown, VA, USA, 2015.

[35] H. Zhou, J. Laval, A. Zhou, Y. Wang, W. Wu, Z. Qing, and S. Peeta, "Review of learning-based longitudinal motion planning for autonomous vehicles: Research gaps between self-driving and traffic congestion," 2019, *arXiv:1910.06070*.

[36] R. F. Tomás, P. Fernandes, E. Macedo, J. M. Bandeira, and M. C. Coelho, "Assessing the emission impacts of autonomous vehicles on metropolitan freeways," *Transp. Res. Proc.*, vol. 47, pp. 617–624, Jan. 2020, doi: 10.1016/j.trpro.2020.03.139.

[37] E. Aria, J. Olstam, and C. Schwietering, "Investigation of automated vehicle effects on driver's behavior and traffic performance," *Transp. Res. Proc.*, vol. 15, pp. 761–770, Jan. 2016, doi: 10.1016/j.trpro.2016.06.063.

[38] H. Chin, H. Okuda, Y. Tazaki, and T. Suzuki, "Model predictive cooperative cruise control in mixed traffic," in *Proc. 41st Annu. Conf. IEEE Ind. Electron. Soc. (IECON)*, Nov. 2015, pp. 3199–3205, doi: 10.1109/IECON.2015.7392593.

[39] M. M. Morando, Q. Tian, L. T. Truong, and H. L. Vu, "Studying the safety impact of autonomous vehicles using simulation-based surrogate safety measures," *J. Adv. Transp.*, vol. 2018, Apr. 2018, Art. no. 6135183.

[40] S. M. Mousavi, O. A. Osman, D. Lord, K. K. Dixon, and B. Dadashova, "Investigating the safety and operational benefits of mixed traffic environments with different automated vehicle market penetration rates in the proximity of a driveway on an urban arterial," *Accident Anal. Prevention*, vol. 152, Mar. 2021, Art. no. 105982, doi: 10.1016/j.aap.2021.105982.

[41] A. Karbasi and S. O'Hern, "Investigating the impact of connected and automated vehicles on signalized and unsignalized intersections safety in mixed traffic," *Future Transp.*, vol. 2, no. 1, pp. 24–40, Jan. 2022, doi: 10.3390/futuretransp2010002.

[42] J. Zhu, S. Easa, and K. Gao, "Merging control strategies of connected and autonomous vehicles at freeway on-ramps: A comprehensive review," *J. Intell. Connected Vehicles*, vol. 5, no. 2, pp. 99–111, 2022, doi: 10.1108/jicv-02-2022-0005.

[43] T. Nishi, P. Doshi, and D. Prokhorov, "Merging in congested freeway traffic using multipolicy decision making and passive actor-critic learning," *IEEE Trans. Intell. Vehicles*, vol. 4, no. 2, pp. 287–297, Jun. 2019, doi: 10.1109/TIV.2019.2904417.

[44] H. Okuda, T. Suzuki, K. Harada, S. Saigo, and S. Inoue, "Quantitative driver acceptance modeling for merging car at highway junction and its application to the design of merging behavior control," *IEEE Trans. Intell. Transp. Syst.*, vol. 22, no. 1, pp. 329–340, Jan. 2021, doi: 10.1109/TITS.2019.2957391.

[45] J. Liu, W. Zhao, and C. Xu, "An efficient on-ramp merging strategy for connected and automated vehicles in multi-lane traffic," *IEEE Trans. Intell. Transp. Syst.*, vol. 23, no. 6, pp. 5056–5067, Jun. 2022, doi: 10.1109/TITS.2020.3046643.

[46] S. Karbalaieali, O. A. Osman, and S. Ishak, "A dynamic adaptive algorithm for merging into platoons in connected automated environments," *IEEE Trans. Intell. Transp. Syst.*, vol. 21, no. 10, pp. 4111–4122, Oct. 2020, doi: 10.1109/TITS.2019.2938728.

[47] R. Balakrishna, C. Antoniou, M. Ben-Akiva, H. N. Koutsopoulos, and Y. Wen, "Calibration of microscopic traffic simulation models: Methods and application," *Transp. Res. Rec., J. Transp. Res. Board*, vol. 1999, no. 1, pp. 198–207, Jan. 2007.

[48] M. Jha, G. Gopalan, A. Garms, B. P. Mahanti, T. Toledo, and M. E. Ben-Akiva, "Development and calibration of a large-scale microscopic traffic simulation model," *Transp. Res. Rec., J. Transp. Res. Board*, vol. 1876, no. 1, pp. 121–131, Jan. 2004.

[49] A. Paz, V. Molano, and C. Gaviria, "Calibration of CORSIM models considering all model parameters simultaneously," in *Proc. 15th Int. IEEE Conf. Intell. Transp. Syst.*, Sep. 2012, pp. 1417–1422.

[50] J. Ma, H. Dong, and H. M. Zhang, "Calibration of microsimulation with heuristic optimization methods," *Transp. Res. Rec., J. Transp. Res. Board*, vol. 1999, no. 1, pp. 208–217, Jan. 2007, doi: 10.3141/1999-22.

[51] C. Cobos, C. Daza, C. Martínez, M. Mendoza, C. Gaviria, C. Arteaga, and A. Paz, "Calibration of microscopic traffic flow simulation models using a memetic algorithm with solis and wets local search chaining (MA-SW-Chains)," in *Advances in Artificial Intelligence (IBERAMIA)* (Lecture Notes in Computer Science), vol. 10022. Cham, Switzerland: Springer, Nov. 2016, pp. 365–375, doi: 10.1007/978-3-319-47955-2.

[52] L. Li, X. D. Chen, and L. Zhang, "A global optimization algorithm for trajectory data based car-following model calibration," *Transp. Res. C, Emerg. Technol.*, vol. 68, pp. 311–332, Jul. 2016, doi: 10.1016/j.trc.2016.04.011.

[53] P. G. Gipps, "A behavioural car-following model for computer simulation," *Transp. Res. B, Methodol.*, vol. 15, no. 2, pp. 105–111, 1981, doi: 10.1016/0191-2615(81)90037-0.

[54] R. Jiang, Q. Wu, and Z. Zhu, "Full velocity difference model for a car-following theory," *Phys. Rev. E, Stat. Phys. Plasmas Fluids Relat. Interdiscip. Top.*, vol. 64, no. 1, pp. 2–5, Jun. 2001, doi: 10.1103/PhysRevE.64.017101.

[55] H. U. Ahmed, Y. Huang, and P. Lu, "A review of car-following models and modeling tools for human and autonomous-ready driving behaviors in micro-simulation," *Smart Cities*, vol. 4, no. 1, pp. 314–335, Mar. 2021, doi: 10.3390/smartcities4010019.

[56] K. Nishinari, "Traffic flow dynamics: Data, models and simulation," *Phys. Today*, vol. 67, no. 3, p. 54, Mar. 2014, doi: 10.1063/PT.3.2314.

[57] M. Treiber, A. Hennecke, and D. Helbing, "Congested traffic states in empirical observations and microscopic simulations," *Phys. Rev. E, Stat. Phys. Plasmas Fluids Relat. Interdiscip. Top.*, vol. 62, no. 2, pp. 1805–1824, Aug. 2000, doi: 10.1103/PhysRevE.62.1805.

[58] J. A. Laval and C. F. Daganzo, "Lane-changing in traffic streams," *Transp. Res. B, Methodol.*, vol. 40, no. 3, pp. 251–264, Mar. 2006, doi: 10.1016/j.trb.2005.04.003.

[59] P. Hidas, "Modelling vehicle interactions in microscopic simulation of merging and weaving," *Transp. Res. C, Emerg. Technol.*, vol. 13, no. 1, pp. 37–62, Feb. 2005, doi: 10.1016/j.trc.2004.12.003.

[60] H. Wei, J. Lee, Q. Li, and C. J. Li, "Observation-based lane-vehicle assignment hierarchy: Microscopic simulation on urban street network," *Transp. Res. Rec., J. Transp. Res. Board*, vol. 1710, no. 1, pp. 96–103, Jan. 2000, doi: 10.3141/1710-11.

[61] K. Nagel, D. E. Wolf, P. Wagner, and P. Simon, "Two-lane traffic rules for cellular automata: A systematic approach," *Phys. Rev. E, Stat. Phys. Plasmas Fluids Relat. Interdiscip. Top.*, vol. 58, no. 2, pp. 1425–1437, Aug. 1998.

[62] X. Hu, Z. Zheng, D. Chen, X. Zhang, and J. Sun, "Processing, assessing, and enhancing the Waymo autonomous vehicle open dataset for driving 1065 behavior research," *Transp. Res. C, Emerg. Technol.*, vol. 134, Jan. 2022, Art. no. 103490, doi: 10.1016/j.trc.2021.103490.

[63] D. R. Jones, "The DIRECT global optimization algorithm," in *Encyclopaedia of Optimization*. Boston, MA, USA: Springer, 2019, pp. 431–440, doi: 10.1007/978-0-387-74759-0.

[64] D. R. Jones, C. D. Perttunen, and B. E. Stuckman, "Lipschitzian optimization without the Lipschitz constant," *J. Optim. Theory Appl.*, vol. 79, no. 1, pp. 157–181, Oct. 1993, doi: 10.1007/BF00941892.

[65] Q. Lu, T. Tettamanti, D. Hörcher, and I. Varga, "The impact of autonomous vehicles on urban traffic network capacity: An experimental analysis by microscopic traffic simulation," *Transp. Lett.*, vol. 12, no. 8, pp. 540–549, Sep. 2020, doi: 10.1080/19427867.2019.1662561.

[66] B. van Arem, C. J. G. van Driel, and R. Visser, "The impact of cooperative adaptive cruise control on traffic-flow characteristics," *IEEE Trans. Intell. Transp. Syst.*, vol. 7, no. 4, pp. 429–436, Dec. 2006, doi: 10.1109/TITS.2006.884615.

[67] L. Zhao and J. Sun, "Simulation framework for vehicle platooning and car-following behaviors under connected-vehicle environment," *Proc.-Social Behav. Sci.*, vol. 96, pp. 914–924, Nov. 2013, doi: 10.1016/j.sbspro.2013.08.105.

PRANAV RAMSAHYE received the B.Eng. degree (Hons.) in civil engineering from Monash University Malaysia, Bandar Sunway, Malaysia, in 2020. He was a Research Assistant with the School of Engineering, Monash University Malaysia. His current research interests include the traffic microsimulation of automated vehicles and automated vehicle control.

SUSILAWATI SUSILAWATI (Member, IEEE) received the B.Eng. degree from Gadjah Mada University (UGM), Indonesia, in 2001, and the master's and Ph.D. degrees in transportation engineering from the University of South Australia, in 2007 and 2012, respectively.

From 2001 to 2006, she was a Spatial Analyst with Caltex Indonesia and Black and Veatch Indonesia. From 2012 to 2013, she was a Senior Spatial Analyst with the South Australia Health Department. Since 2014, she has been with Monash University Malaysia. She is currently a Senior Lecturer with the Department of Civil Engineering, Monash University Malaysia. Her current research interests include intelligent transportation systems and connected and automated vehicle environments. She is a member and a Chartered Professional Engineer of the Engineering Australia (EA). She was a recipient of the Australian Road Research Board (ARRB) Young Researcher, in 2010.

CHEE PIN TAN (Senior Member, IEEE) received the B.Eng. degree (Hons.) in electrical and electronics and the Ph.D. degree in engineering from the University of Leicester, Leicester, U.K., in 1998 and 2002, respectively. He is currently a Professor with the School of Engineering, Monash University Malaysia, Bandar Sunway, Malaysia. He has authored or coauthored more than 60 internationally peer-reviewed research articles, including a book on fault reconstruction. His current research interests include robust fault estimation and observers. He is an Associate Editor of IEEE TRANSACTIONS ON CYBERNETICS, *Journal of the Franklin Institute*, and the *International Journal of Systems Science*.

MD ABDUS SAMAD KAMAL (Senior Member, IEEE) received the B.Sc.Eng. degree from the Khulna University of Engineering and Technology (KUET), Bangladesh, in 1997, and the master's and Ph.D. degrees from Kyushu University, Japan, in 2003 and 2006, respectively.

He was a Lecturer with KUET, from 1997 to 2000; a Researcher with Kyushu University, in 2006 and from 2008 to 2011; an Assistant Professor with International Islamic University Malaysia, Malaysia, from 2006 to 2008; a Researcher with The University of Tokyo, Japan; and a Researcher with the Japan Science and Technology Agency, Japan, from 2011 to 2014. He was a Visiting Researcher with Toyota Central Research and Development Laboratories Inc., Japan, from 2014 to 2016. He was a Senior Lecturer with the School of Engineering, Monash University Malaysia, from 2016 to 2019. He is currently an Associate Professor with the Graduate School of Science and Technology, Gunma University, Japan. His current research interests include intelligent transportation systems, connected and automated vehicle environments, and model predictive control applications.